Efficient quasi-kinematic large-scale dynamo as the small-scale dynamo saturates

Pallavi Bhat,[1, 2, 3, *] Kandaswamy Subramanian,[4] and Axel Brandenburg[5, 6, 7, 8]

[1]*International Centre for Theoretical Sciences, Tata Institute of Fundamental Research, Bangalore 560089, India*
[2]*Plasma Science and Fusion Center, Massachusetts Institute of Technology, Cambridge, MA 02139, USA*
[3]*Department of Applied Mathematics, University of Leeds, Leeds, LS2 9JT, UK*
[4]*IUCAA, Post Bag 4, Ganeshkhind, Pune 411007, India*
[5]*Nordita, KTH Royal Institute of Technology and Stockholm University, SE-10691 Stockholm, Sweden*
[6]*The Oskar Klein Centre, Department of Astronomy, Stockholm University, SE-10691 Stockholm, Sweden*
[7]*McWilliams Center for Cosmology & Department of Physics, Carnegie Mellon University, PA 15213, USA*
[8]*School of Natural Sciences and Medicine, Ilia State University, 0194 Tbilisi, Georgia*

(Dated: April 15, 2022, Revision: 1.149)

Large-scale magnetic fields in stars and galaxies are thought to arise by mean-field dynamo action due to the combined influence of both helical turbulence and shear. Those systems are also highly conducting and the turbulence therein leads to a fluctuation (or small-scale) dynamo which more rapidly amplifies magnetic field fluctuations on the eddy scales and smaller. Will this then interfere with and suppress the mean (or large-scale) field growth? Using direct numerical simulations of helical turbulence (with and without shear), we identify a novel quasi-kinematic large-scale dynamo which operates as the small-scale dynamo saturates. Thus both dynamos operate efficiently, one after the other, and lead to the generation of significant large-scale fields.

Magnetic fields coherent on large-scales, larger than the scales of turbulent motions in the system, are prevalent in stars and disk galaxies. Their origin is thought to lie in mean-field or large-scale dynamo (LSD) action due to helical turbulence often combined with shear. Turbulence in stars and galaxies also has a very high magnetic Reynolds number Re_M. This generically leads to a fluctuation or small-scale dynamo (SSD) which grows random and small-scale magnetic fields more rapidly [1, 2]. Here, small scales correspond to scales smaller than the outer scale of the turbulence.

In large Re_M helical turbulence, previous work has shown that, while the kinematic phase is dominated by rapidly growing small-scale fields [3], there are hints of large-scale field growth [4]. A unified dynamo grows magnetic fields in the kinematic regime, of both large and small scales, with a shape-invariant eigenfunction [4, 5]. The saturation of the unified dynamo occurs first at small scales, and then at progressively larger scales [5, 6]. Significant large-scale fields tend to arise, but on long resistive time scales due to nonlinear growth governed by the slow resistive decay of small-scale helicity [7]. **A matter of outstanding concern is whether large-scale fields can be grown unhindered by rapidly growing small-scale fields via a fast dynamo action [8, 9].**

In this work, we use helically forced turbulence with uniform shear (and sometimes without) to identify a novel intermediate second stage of fast growth (an exponential one, possibly modulated by some other function) growing large-scale field, different from that of the kinematic unified dynamo, due to a quasi-kinematic LSD (QKLSD). The term 'quasi-kinematic' is to signify that this LSD action arises as the SSD saturates (indicating that the system has become nonlinear) while the large-scale field is possibly still unaffected by the Lorentz force. This arises in a previously unidentified parameter regime, but one that is in fact expected to be generic in astrophysical systems. This result, that a quasi-kinematic LSD can operate in large Re_M systems, alleviates the long-standing concern that large-scale fields are overwhelmed by rapidly growing small-scale fields in such systems. **Note that this work is limited to the 'quasi-kinematic' regime and does not deal with the nonlinear issue of catastrophic quenching.**

For reasons of computational efficiency, we solve the equations for a compressible gas; see [10] for a more detailed motivation. We employ a periodic or shearing-periodic domain of size L^3 with $L = 2\pi$, so the smallest wavenumber is $k_1 = 2\pi/L = 1$. We follow a setup similar to that of Ref. [5], except now we also have cases with uniform linear shear. All simulations (except one) were performed with the PENCIL CODE [11], and have a resolution of 512^3 and a magnetic Prandtl number of $\mathrm{Pr}_\mathrm{M} = 10$. **The ability of numerical codes to conserve magnetic helicity has been recognized and was verified on earlier occasions [12].** We have specified the relevant parameters for each run in Table I. Turbulence is driven at the forcing wave number of $k_\mathrm{f}/k_1 = 4$ (or 8 in one case). The unit of velocity is the sound speed c_s, and that of time is $(c_\mathrm{s}k_1)^{-1}$. Also, we have included a run from the paper [13] (referred to as Run GP600Pm1a). This simulation was performed using DEDALUS [14]. The runs leading to LSD action – with shear (like Run A) and without shear (like Run B) – have helical forcing. In the following, we discuss results from these runs and compare with two similar runs (C and D) with non-helical forcing and thus only SSD action.

In the top panel of Fig. 1, we show the evolution of the

* pallavi.bhat@icts.res.in

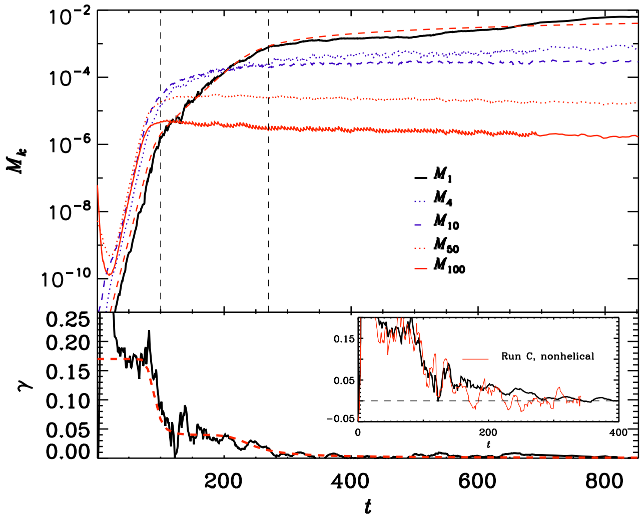

FIG. 1. Evolution of $M_k(t)$ for $k = 1$, 4, 10, 50, and 100 for Run A. The bottom panel shows γ, the growth rate of M_1. The curve in dashed red is from the toy model. The inset compares γ between Runs A and C.

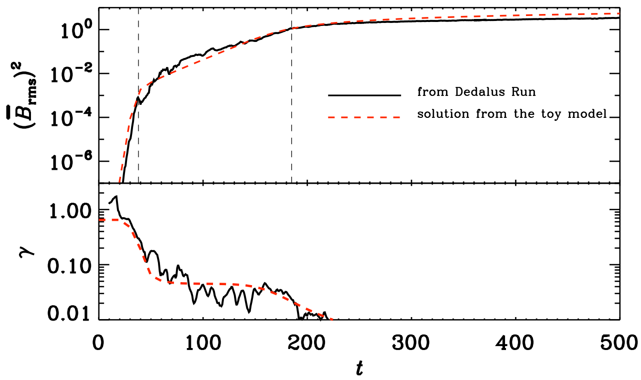

FIG. 2. Evolution of energy in xz averaged field $\overline{\boldsymbol{B}}^2_{\rm rms}$ and γ for Run GP600Pm1a using a different code, DEDALUS [13].

magnetic energy spectrum M_k at certain wave numbers k. We characterize large- and small-scale fields through the magnetic energy at $k < k_{\rm f}$ and $k > k_{\rm f}$, respectively. The quantity M_1 is seen to grow exponentially at the same kinematic rate as others until about $t = 100$. However, there is a novel second phase between $t = 100$ to $t \sim 250$–270, where M_1 grows fast (exponentially, possibly modulated by another function) at a different, albeit slower rate compared to the first stage. Meanwhile all modes with $k \geq k_{\rm f}$ have slowed down towards saturation. The third phase, after $t \sim 300$, involves the well-known resistively limited nonlinear growth of M_1 [7, 15]. For Run A, we have also calculated the large-scale field $\overline{\boldsymbol{B}}_{\rm rms}$ from horizontal or xy averaging and find that its energy density closely follows the M_1 curve. In the top panel of Fig. 2, we show the evolution of $\overline{\boldsymbol{B}}^2_{\rm rms}$ from Run GP600Pm1a with a completely different code using a different forcing function based on the Galloway-Proctor flow with no large-scale shear. We find that the second phase also shows up in this Dedalus run [13], as well as a PENCIL CODE run, Run B where there is no shear.

The bottom panels of Figs. 1 and 2 show the growth rate of the large-scale magnetic energy, defined as $\gamma = d\ln M_1/dt$ or $\gamma = d\ln \overline{\boldsymbol{B}}^2_{\rm rms}/dt$. Two successive stages of fast growth can clearly be identified. The inset in Fig. 1 compares the growth rate of M_1 between the helical and nonhelical cases to illustrate that in the latter, where no LSD action occurs, the curve in the second phase simply fluctuates around $\gamma = 0$, as opposed to the (noisy) plateau in the former case.

In both Figs. 1 and 2 we show, as red-dashed lines, solutions from the following toy model:

$$\mathrm{d}E_{\rm M}/\mathrm{d}t = \left[\frac{\gamma_1 - \gamma_2}{1 + {E_{\rm M}}^2/E_{\rm M1}^2} + \frac{\gamma_2}{1 + {E_{\rm M}}^2/E_{\rm M2}^2}\right] E_{\rm M}. \quad (1)$$

When $E_{\rm M} \ll E_{\rm M1} < E_{\rm M2}$), the growth rate of the curve $E_{\rm M}$ asymptotes to γ_1. Later, when $E_{\rm M1} < E_{\rm M} \ll E_{\rm M2}$, the growth rate asymptotes to γ_2. The overlay from this toy model is found to match quite well both the evolution and growth where the parameters γ_1, γ_2 are the same as the γ calculated from the data.

We propose that the LSD action in the second distinctive phase of growth of the large-scale field is similar to a standard LSD as predicted by mean-field dynamo theory. In the first stage, which is entirely kinematic, the faster SSD is the main driver and thus governs the growth rate of magnetic energy over all scales. Once the growth at smaller scales has slowed down, LSD action becomes prominent. Note that the the magnetic evolution curve in the second stage (QKLSD regime) is not a clean exponential but has a certain concavity. This is attributed to the fact that it is influenced by the transition to or from the other two regimes.

For the following discussion, it is helpful to refer to the standard mean-field equations obtained by splitting the induction equation into one for the mean or large-scale field $\overline{\boldsymbol{B}}$ and the fluctuating or small-scale field $\boldsymbol{b}$ [16],

$$\frac{\partial \overline{\boldsymbol{B}}}{\partial t} = \boldsymbol{\nabla} \times \left(\overline{\boldsymbol{U}} \times \overline{\boldsymbol{B}} + \overline{\boldsymbol{\mathcal{E}}} - \eta \boldsymbol{\nabla} \times \overline{\boldsymbol{B}}\right), \quad (2)$$

$$\frac{\partial \boldsymbol{b}}{\partial t} = \boldsymbol{\nabla} \times \left(\overline{\boldsymbol{U}} \times \boldsymbol{b} + \boldsymbol{u} \times \overline{\boldsymbol{B}} - \eta \boldsymbol{\nabla} \times \mathbf{b} + \mathbf{G}\right). \quad (3)$$

Here $\overline{\boldsymbol{\mathcal{E}}} = \overline{\boldsymbol{u} \times \boldsymbol{b}}$ and $\boldsymbol{G} = \boldsymbol{u} \times \boldsymbol{b} - \overline{\boldsymbol{\mathcal{E}}}$ is a term nonlinear in the fluctuations. The mean velocity accounts for the linear shear, $\overline{\boldsymbol{U}} = (0, Sx, 0)$, where $S = $ const. We also find that helical forcing combined with shear induces a large-scale flow $\overline{\boldsymbol{U}} = (\overline{U}_x(z), \overline{U}_y(z), 0)$ on xy averaging but this does not appear to affect the LSD (see below).

This phenomenon is the vorticity dynamo [17, 18], which is known to be suppressed by the magnetic field [19, 20].

During the kinematic stage, the small-scale field is mainly driven by $\boldsymbol{\nabla}\times(\boldsymbol{u}\times\boldsymbol{b})$, which leads to SSD action. All the terms that depend on averaged or mean quantities are not significant initially. In our simulations, the shearing timescale is much larger than the eddy turn over timescale and thus, its effect on SSD growth is unimportant [21]. The small-scale field then grows exponentially as $\boldsymbol{b}=\boldsymbol{b}_0\exp(\gamma_{\rm SSD}t)$, where $\gamma_{\rm SSD}$ is the SSD growth rate. In Eq. (2), the time evolution of $\boldsymbol{\mathcal{E}}$, which drives $\overline{\boldsymbol{B}}$, is then controlled by the exponentially growing low wave number tail of the small-scale field, given that the velocity field $\boldsymbol{u}$ is in a statistical steady state. The shear term $\boldsymbol{\nabla}\times\left(\overline{\boldsymbol{U}}\times\overline{\boldsymbol{B}}\right)$ is subdominant as $\overline{\boldsymbol{B}}$ is at this stage much smaller than $\boldsymbol{b}$. The rate of change of $\overline{\boldsymbol{B}}$ is therefore expected to be nearly the same as $\gamma_{\rm SSD}$. This can be seen also in Fig. 3, where in the left panel we show that the time evolution of M_1 in both the helical shear dynamo simulations (Run A) and non-helical shear dynamo (Run C) coincide in the kinematic stage. Similarly, in the right panel of Fig. 3, the M_1 curves from the helical dynamo (Run B) and the non-helical dynamo (Run D) coincide. Thus, the kinematic stage is primarily driven by the SSD with $\overline{\boldsymbol{B}}$ being enslaved by $\boldsymbol{b}$.

Eventually, the growth of the small-scale field slows down from an exponential to a more linear form as the SSD begins to saturate. We find this coincides with the QKLSD regime. As seen in the upper panel of Fig. 1, the evolution of M_4 slows down at around $t=100$, when M_1 switches to a different rate of exponential growth. Figure 4 shows explicitly the exponentially growing M_1 versus linearly growing M_4, from Run A.

We can understand the QKLSD regime in the following manner. In Eq. (3), besides the shear and SSD terms, now there are contributions due to those containing mean quantities. In particular, the term $\boldsymbol{\nabla}\times(\boldsymbol{u}\times\overline{\boldsymbol{B}})$, interpreted as the tangling of the large-scale field, is expected to be responsible for additional growth of small-scale fields over and above that when there is no LSD. We show that this is indeed the case in Fig. 4, where the linear growth rate of M_4 in the helical dynamo in Run A is larger than that of the non-helical dynamo (Run C) by a factor of about 8.

At this stage, as the tangling of large-scale field by the turbulent velocity $\boldsymbol{u}$ becomes the more dominant mechanism for growth of small-scale fields $\boldsymbol{b}$, this leads to a correlation between $\boldsymbol{b}$ and $\boldsymbol{u}$, proportional to $\overline{\boldsymbol{B}}$. The emf $\boldsymbol{\mathcal{E}}=\overline{\boldsymbol{u}\times\boldsymbol{b}}$, which then depends on $\overline{\boldsymbol{B}}$, can be estimated in the usual fashion as $\boldsymbol{\mathcal{E}}=\alpha\overline{\boldsymbol{B}}-\eta_{\rm t}\boldsymbol{\nabla}\times\overline{\boldsymbol{B}}$ [16]. Here α and $\eta_{\rm t}$ are the turbulent transport coefficients determining the effect of small-scale turbulence on the large-scale magnetic field. Thus, Eq. (2) for the large-scale field transforms to,

$$\frac{\partial\overline{\boldsymbol{B}}}{\partial t}=\boldsymbol{\nabla}\times\left(\overline{\boldsymbol{U}}\times\overline{\boldsymbol{B}}+\alpha\overline{\boldsymbol{B}}\right)+\eta_{\rm T}\nabla^2\overline{\boldsymbol{B}},\quad \boldsymbol{\nabla}\cdot\overline{\boldsymbol{B}}=0,\quad (4)$$

with $\eta_{\rm T}=\eta+\eta_{\rm t}$. This is the standard mean-field dynamo equation, which has solutions in a periodic box of the form $\overline{\boldsymbol{B}}(\boldsymbol{x},t)=\mathrm{Re}\left[\hat{\boldsymbol{B}}(\boldsymbol{k})\exp(\mathrm{i}\boldsymbol{k}\cdot\boldsymbol{x}+\lambda t)\right]$ at the kinematic stage. For simplicity, assume that the large-scale field varies only along z, so $k_y=k_x=0$. Then the eigenvalue λ is given by [22],

$$\lambda_{\pm}=-\eta_{\rm T}k_z^2\pm\left(\alpha^2k_z^2-\mathrm{i}\alpha Sk_z\right)^{1/2}.\qquad (5)$$

We note that the $\overline{\boldsymbol{U}}$ from the vorticity dynamo does not affect the dispersion relation as $\boldsymbol{\nabla}\times(\overline{\boldsymbol{U}}\times\overline{\boldsymbol{B}})=0$ when

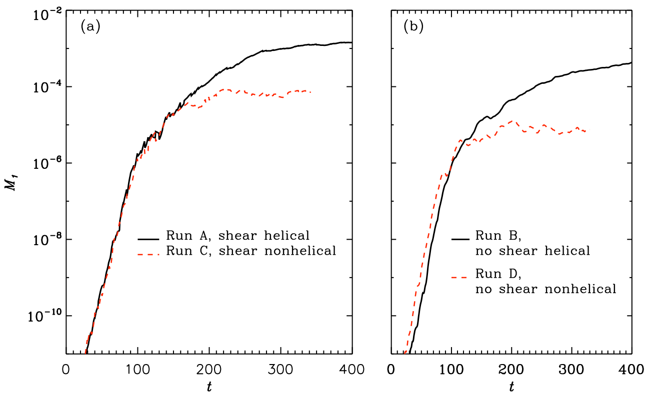

FIG. 3. Comparison of M_1 curves between Runs A and C in the panel (a) and between Runs B and D in the panel (b).

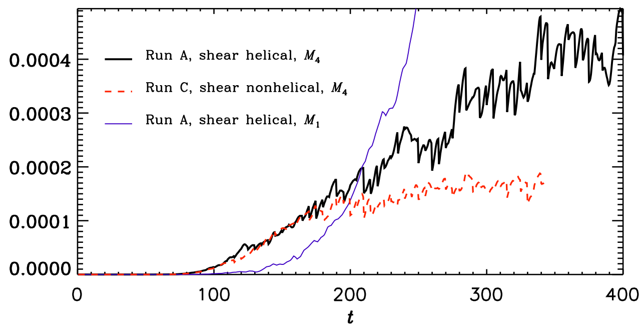

FIG. 4. Comparison of $M_4(t)$ shown for Run A and Run C. Also comparison of curves from Run A – M_1 growing exponentially while M_4 grows linearly.

TABLE I. Summary of all the runs.

Run	$k_{\rm f}$	$u_{\rm rms}$	$S\tau$	forcing	${\rm Re}_{\rm M}$	$\gamma_{\rm theo}$	$\gamma_{\rm meas}$
A	4	0.13	0.38	helical	812	0.11	0.036
B	4	0.18	0	helical	1062	0.12	0.032
C	4	0.13	0.38	non-hel	812	–	–
D	4	0.19	0	non-hel	1187	–	–
E	4	0.10	0.25	helical	1000	0.066	0.026
F	4	0.09	0.11	helical	812	0.034	0.013
G	8	0.09	0.27	helical	281	0.1	0.032
H	4	0.18	0	helical	531	0.12	0.034
GP600Pm1a	8	1.0	0	helical	600	0.22	0.045

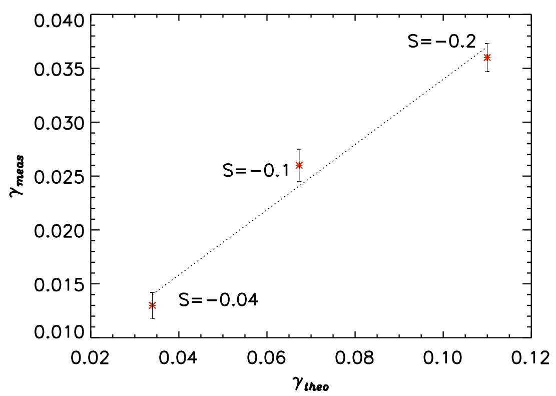

FIG. 5. Comparison between theoretical $\gamma_{\rm theo} = -2\eta_{\rm T}k^2 \pm 2|\frac{1}{2}\alpha S k_z|^{1/2}$ and measured $\gamma_{\rm meas} = d\ln M_1/dt$, for Runs A, E and F (with varying shear, S).

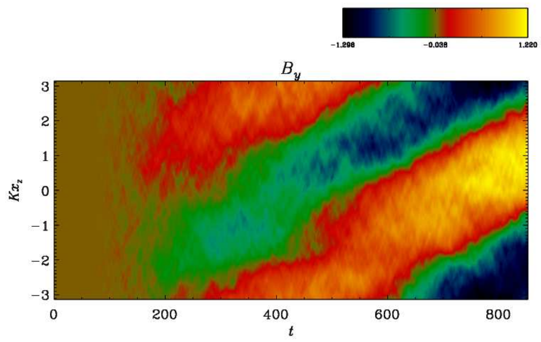

FIG. 6. Space-time diagram where the field components have been xy averaged.

$\overline{B}_z = \overline{U}_z = 0$ and the fields depend only on z. For Run A, the vorticity dynamo becomes suppressed as the magnetic field continues to saturate [23].

For the case without shear (α^2 dynamo), the growing mode has $\lambda = |\alpha|k_z - \eta_{\rm T}k_z^2$. When shear dominates (standard $\alpha\Omega$ dynamo), such that $\alpha k_z/S \ll 1$,

$$\lambda_\pm \approx -\eta_{\rm T}k_z^2 \pm |\tfrac{1}{2}\alpha S k_z|^{1/2}(1-i), \tag{6}$$

We now ask, can the QKLSD growth in Fig. 1, be understood in terms of the above standard mean-field dynamo properties? For homogeneous, isotropic and fully helical turbulence forced at a wave number $k_{\rm f}$, we estimate $\alpha \sim u_{\rm rms}/3$ and $\eta_t \sim u_{\rm rms}/(3k_{\rm f})$ [24]. The real part of the second term (with shear) in Eq. (6) governs the growth rate, while the first term would be smaller in the supercritical case. The magnetic energy density growth rate $\gamma_{\rm theo} = 2{\rm Re}\lambda_+$. In our Run A, $u_{\rm rms} \sim 0.13$, $k_{\rm f} = 4$ and $S\tau \sim 0.38$, which leads to $\gamma_{\rm theo} = 2{\rm Re}\lambda_+ \sim 0.11$, which is larger than the measured value of $\gamma_{\rm meas} \sim 0.036$. This yields an 'efficiency factor' $c_{\rm eff} \sim 0.32$. Note that in the runs with shear, we estimate the $u_{\rm rms}$ after subtracting out $\overline{\boldsymbol{U}}$.

From Eq. (6), we observe that the growth rate is not expected to change much as we change $k_{\rm f}$. We have run a case with $k_{\rm f} = 8$, where $u_{\rm rms} \sim 0.09$ and $S\tau \sim 0.27$, yielding $\gamma_{\rm theo} \sim 0.1$. This theoretical estimate is similar to the $\gamma_{\rm theo}$ of Run A. This is also confirmed by the measurement of the growth rate of ~ 0.032 (similar to the measured value of 0.036 in Run A). In the no-shear case, the theoretical estimate of the growth rate for the large scale magnetic energy is given by $u_{\rm rms}k_{\rm f}/6$ [4]. For Run B, where $u_{\rm rms} \sim 0.18$ this leads to $\gamma_{\rm theo} \sim 0.12$. Here, with $\gamma_{\rm meas} \sim 0.032$, we have $c_{\rm eff} \approx 0.26$. For the run from Dedalus, GP600Pm1a, $u_{\rm rms} \sim 1.$ and $k_{\rm f} \sim 8.5$. We have to account for a factor of 2π considering the the non-dimensionalization of the equations in Dedalus. Thus we find $\gamma_{\rm theo} \sim 0.22$. And with $\gamma_{\rm meas} \sim 0.045$, we have $c_{\rm eff} \approx 0.20$, which is similar to that in runs from Pencil Code, assuring us that the QKLSD regime is robust.

We have varied the shear parameter $S\tau$ to see its effect on the QKLSD growth rate. In Fig. 5, we compare the theoretical estimate of the growth rate for Runs A, E and F (with different values of the shear parameter) against the measured value. We find that $c_{\rm eff}$ is roughly the same in all three cases, thus leading to the points in Fig. 5 falling nearly on a straight line.

Next we examine the oscillatory behavior of the LSD in the runs with shear. In Fig. 6, we show xy averaged field $\overline{B}_y$ in a zt space-time diagram. As in earlier work at lower ${\rm Re}_{\rm M}$ [19], the oscillations begin only during the QKLSD regime. To make an estimate of the time period of this cycle from the mean-field theory, we take ${\rm Re}\lambda_+$ in Eq. (6) to be 0 (which approximately holds as the LSD saturates), and obtain $\omega_{\rm cyc} = \eta_{\rm T}k_z^2$. Thus, the period is $T = 2\pi/\omega_{\rm cyc} = 6\pi(k_{\rm f}/k_1)^2$. For Run A, such an estimate yields $T \sim 300$ and from the simulation shown in Fig. 6, this is the period of the oscillations in the large-scale field. It appears that the mean-field theory is satisfactorily applicable to understand these features of the QKLSD.

A caveat is that we are applying kinematic mean-field theory to a system which is already affected by the Lorentz force. The zeroth order agreement between the measured growth rate and that estimated from the simple $\alpha\Omega$ dynamo theory is possibly because the nonlinearity has not affected the large scales at this stage yet [8]. Note that the quasi-kinematic LSD here arises upon saturation of the SSD and seems to be in alignment with the 'suppression principle' put forward by Tobias and Cattaneo [25].

An important question is regarding the effects of ${\rm Re}_{\rm M}$ on the QKLSD regime. To check this we have lowered in Run H the ${\rm Re}_{\rm M}$ by a factor of 2 compared to that of Run B, and we find that the growth rate remains the same; see Supplemental Material for details of the third stage governed by helicity evolution and also a fourth phase of nonlinear mode switching. Our simulations are in a parameter regime (manifest in astrophysical systems) which allows for separation in large-scale field growth time scales between the three stages. This makes it possible to identify the QKLSD stage distinctively. An intermediate stage of LSD growth was seen in earlier works; see Fig. 8 of Ref. [26] and Fig. 2 of Ref. [27], but was not investigated in detail.

In conclusion, we have demonstrated via direct numerical simulations the presence of a novel second stage growth of large-scale field (QKLSD regime), one that occurs between the kinematic stage driven by the SSD and the saturation stage driven by magnetic helicity decay. Interestingly, we find that the QKLSD growth sets in when the SSD slows down. Our detailed analysis suggests that the classical mean-field theory applies reasonably well to understanding the large-scale field characteristics such as growth rate and frequency of oscillations. Moreover, the growth of the large-scale field in the QKLSD regime seems to be independent of $\mathrm{Re_M}$. Our work thus gives the first detailed evidence for how an LSD operates quasi-kinematically once the small-scale field has saturated and develops an identity even amidst strong small-scale fields.

We thank Anvar Shukurov and Steve Tobias for helpful suggestions. PB thanks Nuno F. Loureiro for support under NSF-DOE award No. DE-SC0016215. This project was completed using funding from the European Research Council (ERC) under the European Union's Horizon 2020 research and innovation programme (grant agreement no. D5S-DLV-786780). This work was supported through the the Swedish Research Council, grant 2019-04234. The simulations in the paper were performed on the MIT-PSFC partition of the Engaging cluster at the MGHPCC facility (www.mghpcc.org), which is funded by DoE grant number DE-FG02-91-ER54109. Additional simulations were performed using resources provided by the Swedish National Infrastructure for Computing (SNIC) at the Royal Institute of Technology in Stockholm.

[1] A. P. Kazantsev, JETP **53**, 1807 (1967), (English translation: Sov. Phys. JETP, 26, 1031–1034, 1968).
[2] R. M. Kulsrud and S. W. Anderson, ApJ **396**, 606 (1992).
[3] S. I. Vainshtein and F. Cattaneo, ApJ **393**, 165 (1992).
[4] K. Subramanian and A. Brandenburg, MNRAS **445**, 2930 (2014), arXiv:1408.4416.
[5] P. Bhat, K. Subramanian, and A. Brandenburg, MNRAS **461**, 240 (2016), arXiv:1508.02706.
[6] F. Rincon, Journal of Plasma Physics **85**, 205850401 (2019), arXiv:1903.07829 [physics.plasm-ph].
[7] A. Brandenburg, ApJ **550**, 824 (2001), astro-ph/0006186.
[8] K. Subramanian, MNRAS **294**, 718 (1998), astro-ph/9707280.
[9] S. M. Tobias, Journal of Fluid Mechanics **912**, P1 (2021), arXiv:1907.03685 [physics.flu-dyn].
[10] X.-Y. Li, G. Svensson, A. Brandenburg, and N. E. L. Haugen, Atmospheric Chemistry & Physics **19**, 639 (2019), arXiv:1806.10529 [physics.ao-ph].
[11] DOI:10.5281/zenodo.2315093, github.com/pencil-code.
[12] A. Brandenburg and E. Scannapieco, ApJ **889**, 55 (2020), arXiv:1910.06074 [astro-ph.SR].
[13] P. Bhat, MNRAS (2021), 10.1093/mnras/stab3138, arXiv:2108.08740 [astro-ph.SR].
[14] K. J. Burns, G. M. Vasil, J. S. Oishi, D. Lecoanet, and B. P. Brown, Physical Review Research **2**, 023068 (2020), arXiv:1905.10388 [astro-ph.IM].
[15] F. Cattaneo, D. W. Hughes, and J.-C. Thelen, Journal of Fluid Mechanics **456**, 219 (2002).
[16] H. K. Moffatt, *Magnetic Field Generation in Electrically Conducting Fluids* (Cambridge University Press, Cambridge, 1978).
[17] T. Elperin, N. Kleeorin, and I. Rogachevskii, PRE **68**, 016311 (2003), astro-ph/0301264.
[18] P. J. Käpylä, D. Mitra, and A. Brandenburg, PRE **79**, 016302 (2009), arXiv:0810.0833.
[19] P. J. Käpylä and A. Brandenburg, ApJ **699**, 1059 (2009), arXiv:0810.2298.
[20] C. Guervilly, D. W. Hughes, and C. A. Jones, Journal of Fluid Mechanics **815**, 333 (2017), arXiv:1607.00824 [physics.flu-dyn].
[21] N. K. Singh, I. Rogachevskii, and A. Brandenburg, ApJ **850**, L8 (2017), arXiv:1610.07215 [astro-ph.SR].
[22] A. Brandenburg and K. Subramanian, PhR **417**, 1 (2005a), arXiv:astro-ph/0405052.
[23] See Supplemental Material, which includes Refs. [10-11], regarding the suppression of the vorticity dynamo by the magnetic field.
[24] S. Sur, A. Brandenburg, and K. Subramanian, MNRAS **385**, L15 (2008), arXiv:0711.3789.
[25] S. M. Tobias and F. Cattaneo, Natur **497**, 463 (2013).
[26] P. J. Käpylä, M. J. Korpi, and A. Brandenburg, A&A **491**, 353 (2008), arXiv:0806.0375.
[27] J. Pietarila Graham, E. G. Blackman, P. D. Mininni, and A. Pouquet, PRE **85**, 066406 (2012), arXiv:1108.3039 [physics.flu-dyn].